Proceedings of SPIE **1998**, 3273, 203-205

STM-electroluminescence probes of metallic and polymeric materials

Yish-Hann Liau and Norbert F. Scherer*

Department of Chemistry and James Franck Institute, University of Chicago
5735 S. Ellis Ave., Chicago, IL 60637

ABSTRACT

The STM-electroluminescence technique is shown to be a valuable tool for characterizing optoelectronic properties and understanding structure-function relationships in heterogeneous or disordered materials on nanometer length scales. The intensity of photon emission induced by tunneling electrons from rough Au films is found to depend on the surface feature size. This size-dependent photon emission yield is shown to agree with the theoretically predicted trend based on the inelastic electron tunneling mechanism. Correlated STM "topography" and electroluminescence measurement of polypyridine (PPy) showed electroluminescence almost exclusively results from low conductivity regions of the film. This anomalous correlation between STM topography and photon emission maps of PPy films is interpreted as the consequence of the spatial variation of the carrier mobility. The results have important implications for understanding the underlying physics of electroluminescence of polymer films as well as for development of optoelectronic devices based on polymeric materials.

Keyword: scanning tunneling microscopy, inelastic electron tunneling, surface plasmons, electroluminescence, nanosphere lithography, polypyridine, Au films.

1. INTRODUCTION

Scanning tunneling microscopes[1] operating in constant current mode not only generate surface topographies with remarkable resolution by recording the feedback voltages of the Z-axis piezo, but also simultaneously provide a microscopic electron source of constant intensity through the few nanometer size tip apex. As a result, by combining scanning tunneling microscopes with photon detecting systems one can study the relation between electron-induced photon emission and local surface structure on atomic and mesoscopic size scales.[2]

Gimzewski and coworkers reported the first STM-induced photon emission results from metals (i.e. Ag films)[2] and more recently showed variations in emission yield correlated with atomic spacings in the metallic lattice.[3] Since then the issue of photon emission resulting from the STM-metallic surface interaction has attracted considerable experimental and theoretical interest. The experiments were mainly concerned with the spectroscopic characterization of tunneling junctions and understanding how the experimental parameters such as the polarity and magnitude of bias voltages affect photon emission.[2-10] On the other hand, the mechanism of photon emission and prediction of spectra were the major emphasis of recent theoretical studies.[11-14] Despite the considerable effort made on this problem controversies still exist on the excitation mechanism of photon emission from rough metal surfaces due to a lack of direct correlation of emission yield with mesoscopic surface morphology.

Surface plasmons, propagating electromagnetic waves, are known to be sensitive to local geometric conditions of surfaces.[15,16] Previous studies have shown that surface plasmon resonances are responsible for the dramatic enhancement of Raman scattering[17] and the enhancement of photoelectron emission from rough metal surfaces.[18,19] Even the mechanism of

photon emission from a metal-insulator-metal tunneling junction was suggested to result from radiative decay of a surface plasmon that was excited by inelastic electron tunneling.[20] Along this line, Persson and Baratoff recently proposed a theory of photon emission in electron tunneling to metallic particles.[14] The metallic particle emitting radiation is modeled by a radiative (dipole) surface plasmon mode. Based on their estimates the two surface plasmon excitation mechanisms, inelastic electron tunneling and hot electron relaxation, can be differentiated by the magnitude and feature size dependence of emission yield. Their work, though based on a simple model, provides analytical expressions of photon emission associated with the mechanisms for STM-induced emission.

STM-induced photon emission experiments are used here to study rough Au films with the purpose of definitively establishing the mechanism of STM-stimulated photon emission induced by the tunneling electrons. The experimental findings and theoretical analysis show that: 1) STM topographic images and photon maps possess spatial correlation on nanometer length scales, 2) the absolute emission probability of rough Au films is consistent with the theoretical estimate based on the inelastic tunneling electron-excited surface plasmon model and, most importantly, 3) the experimental results for particle size-dependent emission can be well reproduced by the same model. Thus the experimental results provide direct evidence demonstrating that inelastic electron tunneling is the principal excitation mechanism of radiative surface plasmon modes for nanometer scale features.[21]

Organic electroluminescent polymers have been suggested be a potential substitute of active materials in semiconductors based light emitting devices and electrically-pumped laser.[22-24] The basic configuration of LED is a layer of emissive materials sandwiched by two electrodes. Under a voltage bias, electrons and holes, injected from the opposite electrodes, travel in the applied field until they combine and form a luminescent excited state. Besides the intrinsic photophysical characteristics of the emissive materials, the performance of organic LED's is mainly determined by the following factors: the injection efficiency of carriers from the electrodes, the transport property for carriers in the emissive materials and the kinetic balance of the above processes for the opposite carriers. Efforts in improving the luminescence efficiency which has been done include choices of the electrodes, doping of the emissive materials, treatment of the electrode surfaces, and inserting a charge transport/injection balancing layer. However, ground understanding of the underlying mechanisms governing the luminescent process is still unsatisfactory. It is partially due to the lack of the spatially resolved electroluminescence efficiency at the sub-micron scale that is essential considering that the aforementioned factors are all microscopic in their nature. It has also been shown that the morphology change at the sub-micron scale results in the change of the conductivity and the carrier dynamics[25]. Here, STM-induced luminescence photon detection system is shown to be capable of characterizing the surface structure and the local luminescence properties of emissive polymeric materials on nanometer scale.

2. EXPERIMENTAL

The experimental schematic for STM-induced luminescence studies is shown in Fig. 1. An important capability of the system is to have simultaneous STM tip access to the sample surface and efficient photon detection. With this key consideration in mind, an STM scanner assembly, which consists of a commercial STM head (Digital Instruments, "A"-head) mounted on a three-axis translation stage for coarse control and engagement of the tip, was mounted on the sample plate of an inverted microscope (Zeiss Axiovert 100). An advantage of using an inverted microscope is to facilitate tip alignment and positioning. The configuration is also capable of pre-selecting an interesting area at optical resolution before performing higher resolution imaging with STM. Photons emitted from the tunneling gap defined by the STM tip and the features on the surface were collected by an objective (N.A. = 0.75), and directed to an electrically cooled photon-counting photomultiplier tube (Hamamatsu R-2949 with a dark count rate below10 counts/sec).

The STM was operated in constant current mode in order to insure constant electron intensity and fixed distance between the tip and the sample surface. The Z piezo voltages and photon counts were then recorded relative to the X-Y coordinates and were used to generate topography and photon maps, respectively. Scanning of the X-Y piezos and data acquisition was performed by a personal computer through a DA/AD converter (National Instruments AT-MIO-16X). The feedback control of the Z-piezo was carried out by the STM controller. All samples were studied in ambient conditions.

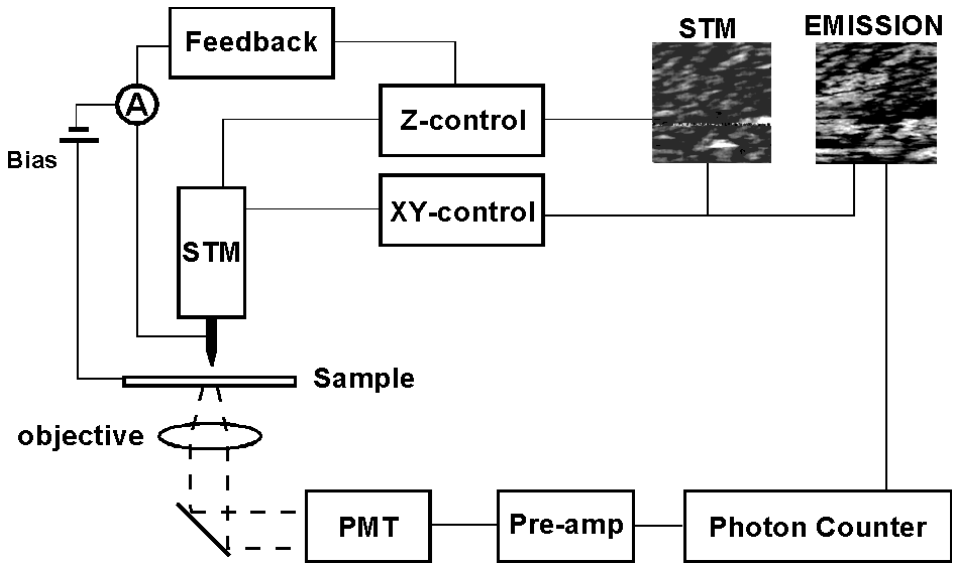

Figure 1 Schematic of the STM-induced luminescence experimental setup. The STM scanner is mounted on the stage of an inverted microscope. The system is housed in an electromagnetic and acoustic isolation enclosure and on a floating vibration isolation table. The symbol containing the "A" represents the current/voltage amplifier.

3. RESULTS AND DISCUSSION

3.1 Rough Au films

The polycrystalline Au rough films were prepared by thermal evaporation of Au onto microscope cover slips. The thickness of the final Au film is about 25 nm as determined by a quartz crystal micro-balance *in situ* to the evaporation process. Due to the statistical character of the thermal evaporation and surface feature growth processes, the resulting surface features range in size from several nm^2 to one thousand nm^2 and can be easily identified in STM images. Fig. 2A shows an STM image of Au polycrystalline films measured at constant current mode. The observed surface roughness determined by AFM and STM measurements are comparable thereby, insuring unambiguous determination of surface feature size in STM images. As many as one hundred features, termed particles, can be identified on the image projecting above the otherwise flat background of the surface. The typical particle sizes range from 20 to 600 angstroms in diameter. Note that the roughness of the glass cover slips has been characterized to be less than 20 angstroms peak-to-peak by AFM; thus the substrates' contribution to the apparent roughness of the Au film is insignificant.

The photon emission map of the same area measured simultaneously with the STM image (Fig. 2A) is shown in Fig. 2B. The two images show similar features. The high emission yield regions generally correlate with the "particles" identified in the STM image. It is noted that the film of Fig.2A (and other not shown) does not emit in a uniform way and that the important length scale of the luminescent regions is on the order of a few hundred angstroms. The close similarity between STM images and photon maps in terms of domain (i.e. "particle") areas and shapes is significant for the analysis performed below because it facilitates the unambiguous identification of the quasi-particles in the STM images with the corresponding emitting domains in the photon maps. The data are analyzed by plotting the emission intensity of each quasi-particle vs. particle radius. A flat background reference surface is established and the protruding area above the reference surface is identified as one particle. The radii of the particles are evaluated by approximating the particles as hemispheres of the same area. The emission intensity of each particle is then obtained by integrating the photon counts within the corresponding emitting domain of the photon map. The results, emission yield vs. particle size for three independent measurements, are plotted in Fig. 3. It is obvious from the figure that the emission yield shows dramatic particle-size dependence. Specifically, the emission is greater as the particle radius increases, reaches a maximum for particle sizes of about 200 angstrom radius and then decreases as the particle size increases further.

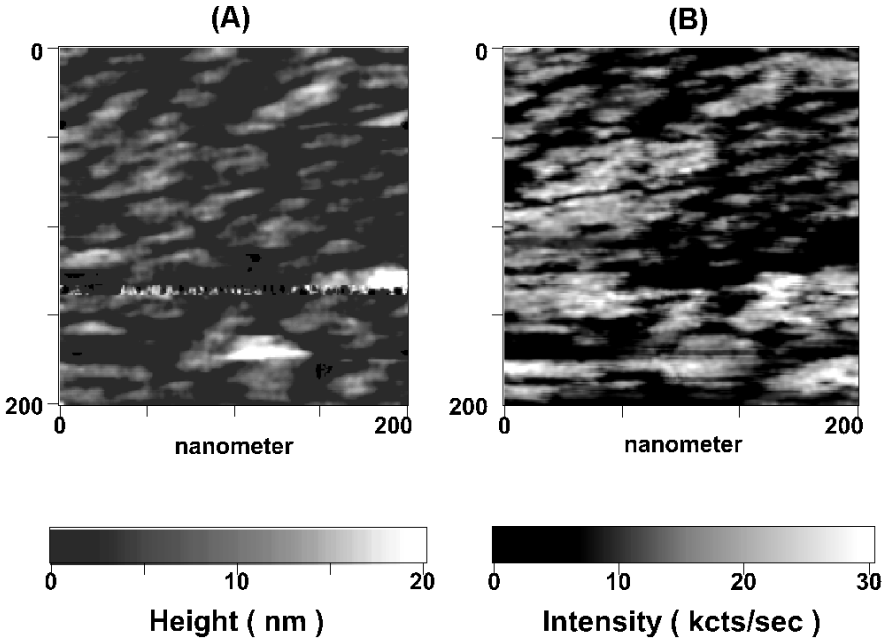

Figure 2(A) STM constant current mode image of a 25 nm thick Au film. The 200 x 200 nm image consists of 40,000 pixels with a scan step size of 1 nm in the X and Y directions. The image was taken in ambient conditions with setpoint tunneling current = 5 nA and bias voltage = 2.5V. (B) Wavelength-integrated photon counting map measured simultaneously with Fig. 2(A).

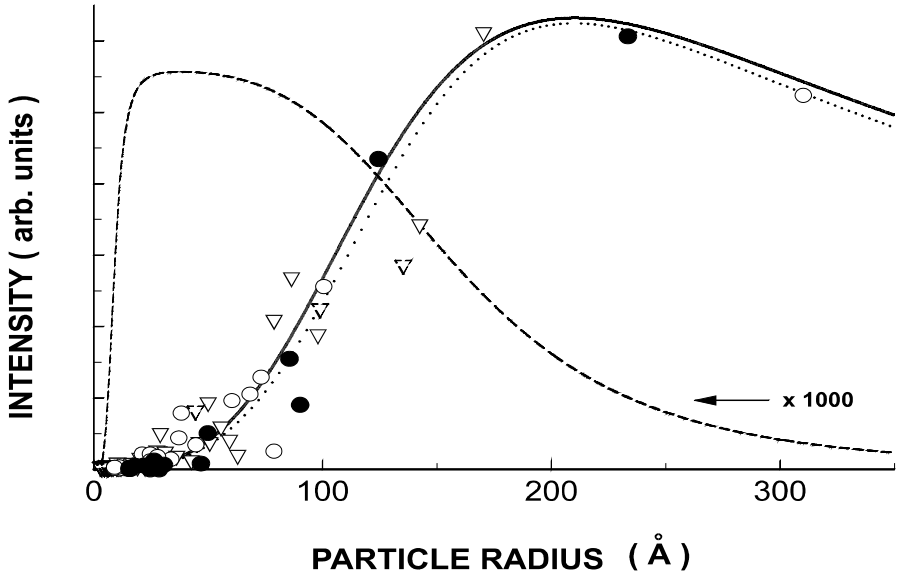

Figure 3 Particle size-dependence of STM-induced photon emission. The solid and dashed lines are the wavelength-integrated emission intensity corresponding to inelastic tunneling and hot electron processes, respectively (see text for detail). Note the dashed line has been multiplied by 1000 for visual comparison. The dotted line is the result of nonlinear least square fitting of Eq. (1) to the data points with $\hbar\Omega = 2\mathrm{eV}$.

The emission probability of the films can be estimated by taking into account the tunneling current setpoint, the optical transmittance of the sample/substrate, the light collection efficiency of the microscope objective, and the quantum efficiency of the PMT, which are 5nA, ~50%, 17%, and ~15% (at 600 nm), respectively. The resultant photon creation probability of Au films is determined to be ~5×10^{-4} photons per tunneling electron. Based on the model for the inelastic tunneling mechanism the theoretically predicted value is ~10^{-3} while the yield associated with the hot-electron mechanism is predicted to be much smaller, of order 10^{-6} .[14]

In order to obtain further insight on the size-dependence of the mechanism for emission observed in STM measurement the theory of Persson and Baratoff[14] is used to evaluate the photon emission probability of metallic particles**.** The photon yield induced by inelastic tunneling associated with a metallic particle of radius R can be expressed as,

$$P_{inelastic}(R) = \left[\frac{\alpha}{8}\right]\left[\frac{\hbar\Omega}{W}\right]\left[\frac{\hbar c / R}{\hbar^2 s^{-2} / 2m}\right]\left[1-\frac{\hbar\Omega}{eV}\right]\left[1+\frac{3\mathrm{C}}{2}\frac{\upsilon_F}{c}\left(\frac{\Omega R}{c}\right)^{-4}\right]^{-1} \quad (1)$$

where $\alpha = \frac{e^2}{\hbar c} \approx \frac{1}{137}$ is the fine-structure constant, e is the electron charge, m is the electron mass, c is the speed of light, s is the separation between the initial and final hybrid states of tunneling electrons extended over the tip and the particle, υ_F is the Fermi velocity, Ω is the resonance frequency of the surface plasmon mode of the metal particle, V is the bias voltage, W is the barrier height and C is a constant.[21] Their equation was extended to conform with the present experimental condition by taking into account the quantum efficiency function of the PMT at various photon energies and a window function defined by the PMT cut-off frequency (1.4eV) and the applied STM bias voltage (2.5V). The solid line in Fig. 3 shows the variation of the emission frequency-integrated photon yield with the particle radius R, assuming s = 6 ○, W = 4 eV, and eV = 2.5 eV. The agreement between the model calculation and the experimental data is excellent considering that no attempt was made to do "curve fitting". If the peak energy of the emission spectrum (2 eV)[4] is chosen and nonlinear regression is performed with respect to the constant C the agreement is only slightly better as shown by the dotted curve in Fig. 3. The good agreement between the experimental and theoretical results provides persuasive evidence that inelastic tunneling is the dominant mechanism responsible for excitation of the radiative surface plasmon modes.

The photon yield associated with the other possible mechanism, the hot electron process, can also be evaluated by considering the two competing decay channels of hot electrons, radiative plasmon decay and non-radiative electron-hole quenching[14] and the result is shown as the dashed line in Fig 3. As pointed out by Barotoff the yield is ~3 orders of magnitude smaller than the emission yield associated with inelastic tunneling mechanism for R ~ 100 - 300 angstroms[14] and thus its contribution to photon emission is negligible in the particle size range considered in the present experiment. Furthermore, the disagreement between the experimental result and the dashed line is obvious even just by inspection. As a result, the possibility of photon emission induced by hot electron injection can be ruled out for several nanometer diameter and larger size particles.

3.2 Structured Au cluster arrays

Our STM-induced photon emission study[21] shows that the photon creation efficiency depends on the size of the particles. It is also believed that the characteristic frequency of the surface plamon modes is also related to the geometry of the particles[14]. Furthermore, due to the propagation property and the long range interaction of the surface plasmon, multiple scattering and interaction between the surface plasmons on different particles are also expected to exist[16] and, consequently, change the emission spectrum.

In order to study the collective response and the interaction of the surface plasmon modes of Au particles, structured Au particle arrays have been fabricated by nanosphere lithography[26,27] The lithography mask is made by a single mono-layer of self-assembled latex spheres which were spin-coated onto Au-coated glass cover slips. A thin layer of Cr (1 nm) has been evaporated onto the cover slips before the deposition of the Au layer to increase the adhesion. The Au layer assures the electrical conduction of the substrate that is necessary for STM imaging. Fig. 4A shows an AFM image of near defect-free hexagonally closed-packed monolayer of latex spheres (dia. 500 nm). Subsequently, the material of interest, Au in this study,

is evaporated over the sphere-coated substrate and, thereby, partially fills into the spacing in between the latex spheres. After deposition of Au the latex spheres were removed by dissolving them in CH_2Cl_2 solvent.

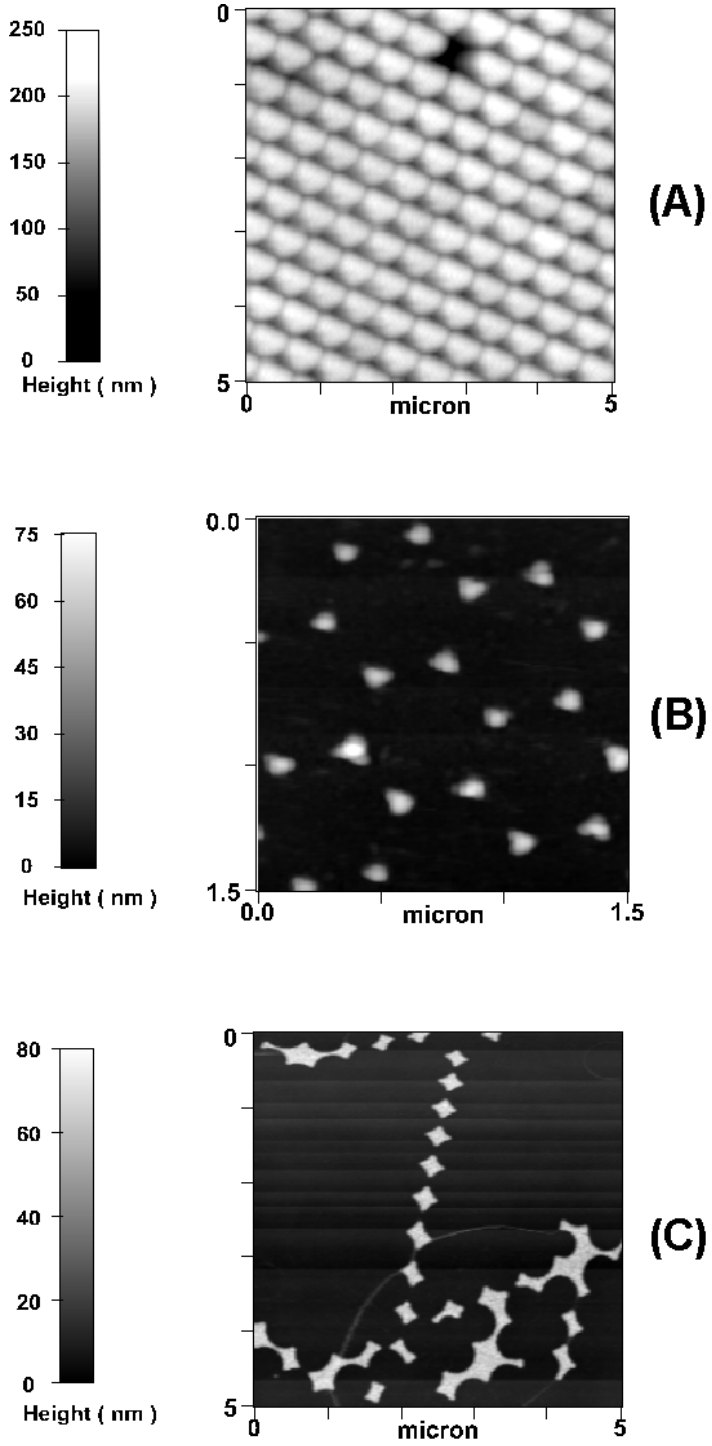

Figure 4 AFM images of (A) self-assembled latex spheres with 500 nm diameter, (B) and (C) nanometer size Au particle arrays made by nanosphere lithography.

Figure 4B and 4C show AFM images of arrays of the nanometer-scale of Au particles left on the flat surface after dissolving of the latex spheres. The height of the Au particles measured by AFM is consistent with the deposition thickness as monitored during the evaporation process. Ideal hexagonal arrays of particles as shown in Fig 4B only occupy in a small portion of the whole area while irregular features as shown in Fig. 4C are more common. It is believed that the particles shown in Fig. 4C are originated from Au filling into the defect areas of close-packed nanospheres by inspection of the shapes of the particles. Work on improving the conditions of fabrication to obtain well controlled patterns is underway. Nevertheless, the particles of various sizes and shapes and the different distances among neighboring particles as shown in Fig 4C still form interesting surface patterns that can be used in study of the aforementioned factors associated with the surface plasmon modes of the metallic materials.

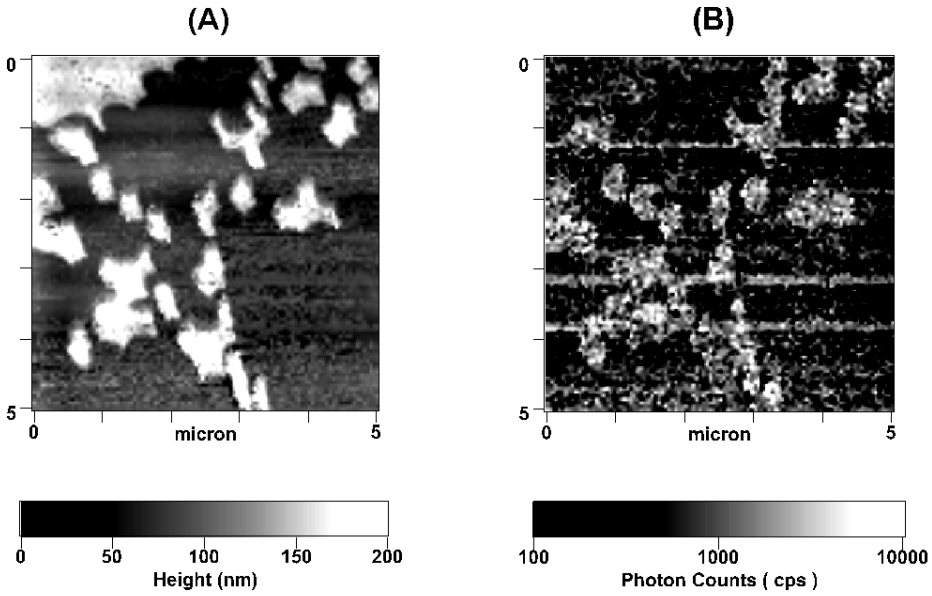

Figure 5(A) STM constant current mode image of Au particle arrays made by nanosphere lithography. The image was taken in ambient conditions with setpoint tunneling current = 1 nA and bias voltage = 2.1V. (B) Wavelength-integrated photon counting map measured simultaneously with Fig. 5(A). The photon intensity is shown by log scale.

Fig. 5A shows the STM topography of the Au particles fabricated by nanosphere lithography. The apparent height of the Au particles in the STM image was found to be greater than the value measured by AFM for the same sample. The reason for the observed anomalous particle height in the STM image is unclear. More work is required to extract real geometric information from the STM measurement.

Fig. 5B is the corresponding photon map recorded simultaneously with the STM measurement shown in Fig. 5A. There is a dramatic difference in emission intensity between the features and the flat surface by two orders of magnitude. The variation of the emission intensity on the top surface of the features is also visible. By comparison of the two images correlation between geometric features and high emission regions is obvious. It is also noted that there is a large feature on the upper left corner with relatively smaller photon yields although the thickness and the surface roughness are expected to be comparable to the other protrusion regions. This indicates that the photon creation efficiency strongly influenced by the size of the features even at the micrometer scale.

A future direction of this work is to study the spectroscopic character of the single features of different geometry and in various neighboring environments in order to elucidate the collective response of surface plasmons of interacting systems.

3.3 Poly-pyridine films

Figure 6A shows a constant current topographic image of PPy films with a scan area of 500 x 500nm. The PPy film was prepared by spin-casting polymer solution onto a transparent ITO-coated cover slip. The sheet resistance of the substrates is about 20 Ω/cm. The bias voltage and setpoint current were chosen to obtain stable STM images and sufficient photon counts for generating a reliable image. Fig. 6B displays the photon map recorded in the same area. The peak luminescence intensity under our experimental condition is about 150 counts/second. The photon creation efficiency per tunneling electron is estimated to be ~ 10^{-6} and is smaller than the emission efficiency of Au films by two orders of magnitude. The size of the luminescent features is on the order of 10 nm and the overall region with detectable luminescence is only a small portion among the whole scanning area. This observation indicates that the luminescence of the polymer is highly non-uniform on the nanometer scale and inefficient. This also implies that there is still considerable room in the improvement of the luminescence efficiency in the development of the optoeletronic devices based on polymeric materials. Furthermore, comparison of the two images shows that the area of highest luminescence generally correlate with "topographically" lower regions in the STM image. The inverse correlation is just opposite to the observation made with the Au rough film. This will be discussed below.

The apparent roughness of the STM topography is noticed to be greater than the roughness of the same sample measured with AFM. Due to the spatial variation of the local conductivity the STM image should only be interpreted as surface topography with care. The tunneling current is known to exponentially relate to the distance between the tip and the sample with a preexpontial factor that is a function of the local electron density of states and the work functions of the tip and the surface[28]. When the STM is operated in constant current mode, the feedback loop tries to maintain a fixed value of tunneling current by adjusting the z-position of the tip. If the local density of states and work function is spatially uniform the tip will track the surface topography and the STM image will represent the geometric topography.

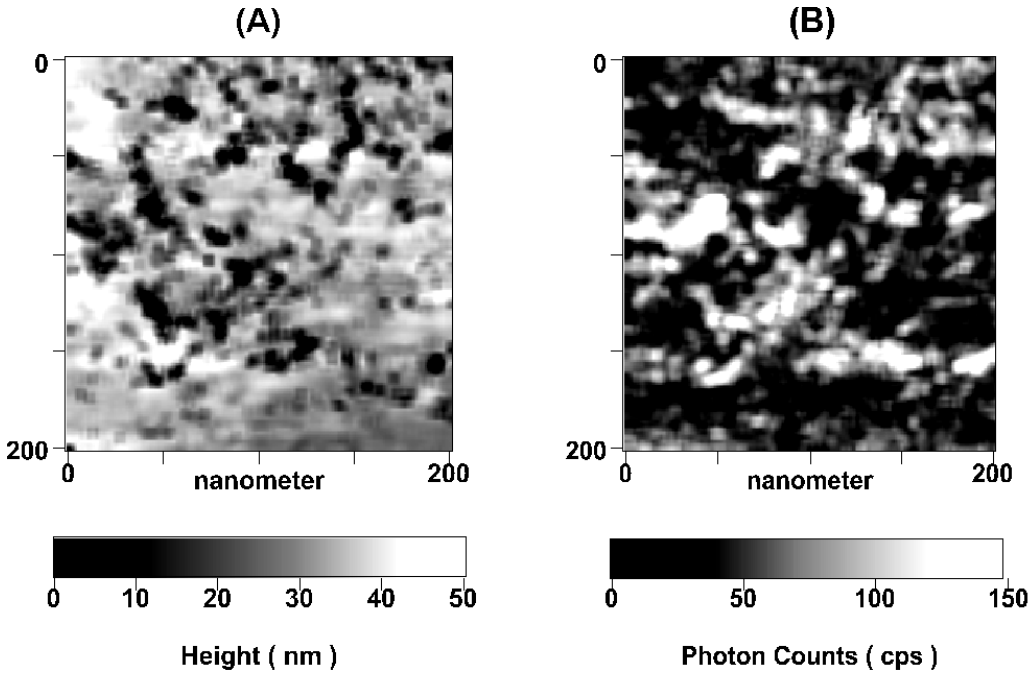

Figure 6(A) STM constant current mode image of poly-pyridine film. The image was taken in ambient conditions with setpoint tunneling current = 5 nA and bias voltage = 7.0V. (B) Wavelength-integrated photon counting map measured simultaneously with Fig. 6(A).

The polymer film consists of coiled polymer chains. The polymer aggregation is thus expected to cause conductivity variation in different areas of the polymer films. Furthermore, the polymer chain is a molecular "wire" that facilitate carrier transport along the chain, that is better than that occurring between chains. As a result, the STM image of the polymer actually represents the combination of the proximity and the local conductivity. The observation that the STM image appears to be much rougher than the AFM image of the same film suggests that the local conductivity rather than the film height dominates the STM image. In other word, the darker areas of the image in Fig. 6A represent low conductivity regions on the film and *vice versa*. Since the Z-axis feedback voltage controls the position of the STM tip, the greater roughness of STM image indicates that the tip probably dips into the film in the low conductivity area in order to approach the counter electrode and thereby achieve the preset tunneling current.

With the above discussion in mind, the observed inverse correlation between the STM image and the luminescence map can be interpreted by considering the spatial variation of the local conductivity. Furthermore, the spatial variation of the carrier mobility is presumed to correlate with the local conductivity. Therefore, in the low conductivity area, i.e. low carrier mobility region, the electrons and holes spend more time in the polymer, or possibly are more likely to be trapped in some site before reaching the opposite electrode. Consequently, the carriers (i.e. electrons and holes) have greater chance for encounter to form the luminescent excitonic state. As a result, we expect to see greater luminescence intensity in low conductivity region. This interpretation is consistent with a common strategy of increasing luminescence efficiency by adding a balancing layer to reduce the mobility of the major carriers and thus balance the charge transport of the opposite carriers[29].

STM-induced electroluminescence of polymer has been reported by other research groups.[30,31] It is noted that in these studies a thin layer of Au film was used as an electrode instead of ITO in our experiment. ITO has been tested to possess no detectable emission under the same experimental condition wherein our studies showed that the photon creation efficiency of the Au films is greater than that of PPy by a factor of ~500. As a result, whether the photon detected is really generated from the polymer sandwiched between the Au electrode and the tip, or is actually emitted from the underlying Au film is questionable. In other words, even though only a small portion of electrons reaching the Au electrode still posses enough energy to excite the plasmon mode of the Au electrode, the emission caused by the radiative decay of Au plasmon modes could dominate the observed emission. In this case, we expect to see normal correlation, i.e. the luminescent features correlate with the conductive region because the electrons reaching the Au electrode are capable of exciting plasmons of the Au electrode. Preliminary results showing the inverse contrast from that shown in Fig. 6 have been obtained with Au STM tip. Still, more work is needed to firmly establish the explanation.

4. CONCLUSION

In summary, an experimental setup based on an STM integrated with photon detection system is shown to be capable of characterizing the optoelectronic properties of various materials including rough Au surfaces, structured Au cluster arrays, and luminescent polymeric films with nanometer resolution and potentially down to molecular resolution. Our studies of rough Au films provide definite evidence that inelastic electron tunneling is the dominant mechanism of photon emission observed in scanning tunneling microscopy measurement. The STM-electroluminescence study of PPy polymer films show that the regions of higher luminescence yields generally correlate with areas of low conductivity. The observed "inverse" correlation between the STM topography and the photon maps for luminescent PPy films can be interpreted as the results of the spatial inhomogeneity of the carrier mobility.

5. ACKNOWLEDGEMENTS

We acknowledge the University of Chicago MRSEC and Packard Foundation for financial support. We also thank Prof. Alan MacDiarmid and Frank Huang for preparing the PPy polymer films studied here.

6. REFERENCES

1. G. Binning, H. Rohrer, C. Gerber, and E. Weibel, ", "Surface studies by scanning tunneling microsciopy" *Phys.Rev.Lett.* **49**, 57 (1982).
2. J.K. Gimzewski, B. Reihl, J.H. Coombs, and R.R. Schlitter, "Photon emission with the scanning tunneling microscope", *Z.Phys.B* **72**, 497 (1988).
3. R. Berndt, R. Gaisch, W.D. Schneider, J.K. Gimzewski, B. Reihl, R.R. Schlitter, and M. Tschudy, "Atomic resolution in photon emission induced by a scanning tunneling microscope", *Phys.Rev.Lett.* **74**, 102 (1995).
4. R. Berndt, J.K. Gimzewski, and P. Johansson, "Inelastic tunneling excitation of tip-induced plasmon modes on noble-metal surfaces", *Phys.Rev.Lett.* **67**, 3796 (1991).
5. I.I. Smolyaninov, V.S. Edelman, and V.V. Zavyalov, "Spectroscopic measurement of light emitted by the scanning tunneling microscope", *Phys.Lett.A* **158,** 337 (1991).
6. V. Sivel, R. Coratger, F. Ajustron, and J. Beauvillain, "Photon emission stimulated by scanning tunneling microscopy in air", *Phys.Rev.B* **45**, 8634 (1992).
7. A.W. McKinnon, M.E. Welland, T.M.H. Wong, and J.K. Gimzewski, "Photon-emission scanning tunneling microscopy of silver films in ultrahigh vacuum: A spectroscopic method", *Phys.Rev.B* **48**, 15250 (1993).
8. R. Berndt, J.K. Gimzewski, and P. Johansson, "Electromagnetic interactions of metallic objective in nanometer proximity", *Phys.Rev.Lett.* **71**, 3493 (1993).
9. V. Sivel, R. Coratger, F. Ajustron, and J. Beauvillain, "Interpretation of the control of the photon emission stimulated by STM", *Phys.Rev.B* **51**, 14598 (1995).
10. T. Umeno, R. Nishitani, A. Kasuya, and Y. Nishina, "Isochromat photon map induced by scanning tunneling microscopy from gold particles", *Phys.Rev.B* **54**, 13499 (1996).
11. P. Johansson, R. Monreal, and P. Apell, "Theory for light emission from a scanning tunneling microscope", *Phys.Rev.B* **42**, 9210 (1990).
12. Y. Uehara, Y. Kimura, S. Ushioda, and K. Takeuchi, "Theory of visible light emission from scanning tunneling microscope", *Jpn.J.Appl.Phys.* **31**, 2465 (1992).
13. A. Madrazo, M. Nieto-Vesperinas, and N. Garcia, "Exact calculation of Maxwell equations for a tip-metallic interface configuration: Application to atomic resolution by photon emission", *Phys.Rev.B* **53**, 3654 (1996).
14. B.N.J. Persson and A. Baratoff, "Theory of photon emission in electron tunneling to metallic particles", *Phys.Rev.Lett.* **68**, 3224 (1992).
15. H. Raether, Springer Tracts in Modern Physics, Vol. 111, "*Surface Plasmons on Smooth and Rough Surfaces and on Gratings"* (Springer, Heidelberg, 1988).
16. W. Wang, M.J. Feldstein, and N.F. Scherer, "Observation of coherent multiple scattering of surface plasmon polariton on Ag and Au surfaces", *Chem.Phys.Lett.* **262**, 573 (1996).
17. C.K. Chen, A.R.B. de Castro, and Y.R. Shen, *Phys.Rev.Lett.* **68**, 476 (1981).
18. M.J. Feldstein, P. Vohringer, W. Wang, and N.F. Scherer, "Femtosecond optical spectroscopy and scanning probe microscopy", *J.Phys.Chem.* **100**, 4739 (1996).
19. C. Douketis, V.M. Shlaev, T.L. Haslett, Z. Wang, and M. Moskovits, "The role of localized surface-plasmon in photoemission from silver films- direct and indirect transition channels", *J.Elec.Spec.Rel.Phen.*, **64/65**, 167 (1993).
20. J. Lambe and S.L. McCarthy, "Light emission from inelastic electron tunneling", *Phys.Rev.Lett.* **37**, 923 (1976).
21. Y.H. Liau and N.F. Scherer, "STM-induced photon emission by inelastic electron tunneling", submitted to *Phys.Rev.Lett*.
22. J.S. Sheats, H. Antoniadis, M. Hueschen, W. Leonard, J. Miller, R. Moon, D. Roitman, and A. Stocking, "Organic electroluminescent devices", *Science*, **273**, 884 (1996).
23. F. Hide, M.A. DiazGarcia, B.J. Schwartz, Q.B. Pei, A.J. Heeger, "Semiconducting polymers: a new class for conjugated-polymer microcavities", *Science*, **273**, 1833 (1996).
24. N. Tessler, G.J. Denton, and R.H. Friend, "Lasing from conjugated-polymer microcavities", *Nature,* **382**, 695, 1996.
25. M. Feldstein, W. Zheng, Y.H. Liau, A.G. MacDiarmid, and N.F. Scherer, "Time-resolved carrier dynamics in polyaniline near the insulator-metal transition", *J.Am.Chem.Soc.,* in press.
26. J.C. Hulteen and R.P. Van Duyne, "Nanosphere lithography: a material general fabrication process for periodic particle array surface", *J.Vac.Sci.Technol. A* **13**, 1553 (1995).
27. M. Winzer, M. Kleiber, N. Dix, and R. Wiesendanger, "Fabrication of nano-dot- and nano-ring-arrays by nanosphere lithography", *Appl. Phys. A* **63**, 617 (1996).
28. C.J. Chen, "*Introduction to scanning tunneling microscopy*", (Oxford, New York, 1993).

29. N.C. Greenham, S.C. Moratti, D.D.C. Bradley, R.H. Friend, and A.B. Holmes, “Efficient light-emitting diodes based on polymer with high electron affinities”, *Nature,* **365**, 628, 1993.
30. D.G. Lidzey, D.D.C. Bradley, S.F. Alvarado, and P.F. Seidler, “Electroluminescence in polymer films”, *Nature,* **386**, 135, 1997.
31. S.F. Alvarado, W. Rieβ, P.F. Seidler, and P. Strohriegl, “STM-induced luminescence study of poly(*p*-phenylenevinylene) by conversion under ultra-clean conditions”, *Phys. Rev. B*, **56**, 1269 (1997)